AIMS Mathematics, 11(6): 17859–17879.
DOI: 10.3934/math.2026728
Received: 20 March 2026
Revised: 03 June 2026
Accepted: 09 June 2026
Published: 18 June 2026

https://www.aimspress.com/journal/Math

*Research article*

# Neurofeedback control of rumor propagation dynamics with cognitive fatigue

**Xiaoyu Miao**[1,2], **Haoran Song**[1] **and Lipu Zhang**[1,2,*]

[1] School of Media Engineering, Communication University of Zhejiang, Hangzhou 310018, China

[2] Zhejiang Key Laboratory of Film and TV Media Technology, Hangzhou 310018, China

* **Correspondence:** Email: zhanglipu@cuz.edu.cn.

**Abstract:** The persistent spread of rumors and misinformation on social media poses severe challenges to public safety. Traditional interventions overlook the idea that repeated debunking induces cognitive fatigue, thus causing diminishing efficiency over time. This paper proposes a novel SHIR-F (Susceptible-Hesitant-Infected-Recovered with Fatigue) dynamic model that incorporates a cognitive fatigue mechanism. By building upon the classical compartmental structure, the model introduces a fatigue state variable and characterizes the diminishing marginal effect of interventions through an exponentially decaying effective debunking efficiency, thereby achieving a quantitative description of public cognitive response mechanisms in information propagation. Regarding the control design, this work constructs a stage-weighted optimal control objective that balances the infection scale against the intervention costs, and develops a closed-loop feedback control strategy parameterized by a dual-branch neural network. This architecture achieves the end-to-end numerical approximation of continuous-time control problems through the collaborative operation of peak and regular branches combined with a fixed-weight fusion mechanism, thus circumventing the computational difficulties associated with solving high-dimensional adjoint equations in traditional Pontryagin methods. A rigorous theoretical analysis proves the positive invariance, global existence, and uniqueness of system solutions, derives explicit expressions for the basic reproduction number, and reveals the monotonic modulation relationship between the fatigue levels and propagation thresholds. Numerical experiments demonstrate that the proposed strategy reduces the infection peaks by 37.4% and the total costs by 48.8%, while ensuring bounded control inputs and fatigue variables, thus exhibiting favorable numerical robustness under parameter perturbation conditions.

**Keywords:** rumor propagation model; cognitive fatigue; SHIR-F system; neurofeedback control; optimal control
**Mathematics Subject Classification:** 34H05, 37N20, 49J15

## 1. Introduction

The spread of rumors and misinformation in social networks has long been modeled as a dynamical process highly analogous to the spread of infectious diseases. Since Daley and Kendall [1] introduced the stochastic rumor model in 1965, the compartmental paradigm has served as a theoretical cornerstone to characterize information diffusion, outbreak, and decline. This class of model divides a population into discrete states such as susceptible, spreaders, and recovered individuals, thereby employing differential equations to describe transitions between these states. The approach has successfully explained exponential growth, threshold effects, and eventual attenuation in rumor propagation [2–5]. Within this framework, researchers subsequently developed extended models that account for topological structures, individual heterogeneity, and media effects, thus enriching the theoretical understanding of rumor mechanisms [6–8].

Cognitive fatigue, as a psychological consequence of information overload, has recently been identified as a critical factor that affects the public information processing capacity. In a cross-cultural study across eight countries, Ahmed and Rasul [9] found a significant positive correlation between social media fatigue and misinformation sharing. Hwang et al. [10] reported that information fatigue increases avoidance behavior and heuristic processing, thus elevating misinformation acceptance. Islam et al. [11] argued from the cognitive load theory that overload-induced fatigue diminishes a users' capacity to judge veracity. Tandoc and Kim [12] identified a bidirectional causal relationship between information overload and news fatigue, while Apuke and Omar [13] confirmed that the cognitive ability moderates the effect of overload on misinformation sharing, with lower-ability individuals being more susceptible. This interdisciplinary body of research suggests that the linear relationship between the debunking efficiency and the control intensity assumed in traditional models may be overly optimistic during long-term interventions, and that cognitive fatigue should be incorporated into the theoretical framework.

To enhance the characterization of realistic propagation, researchers have extended the classical model in several directions. Zhao et al. [14] introduced a hesitant state to depict decision-making hesitation upon encountering rumors; Zhu and Ma [15] analyzed dynamic friendship relationships in heterogeneous SHIR networks. Chen et al. [16] classified individuals by personality traits that affected their rumor credibility perception, and Liu et al. [17] integrated game theory to examine psychological decision-making under equilibrium. Gu et al. [18] and Zhao et al. [19] incorporated time-dependent forgetting and memory recovery, thereby breaking the assumption of constant transition rates and revealing that memory effects alter propagation thresholds. Zanette [4] and Moreno et al. [5] revealed the influence of small-world and scale-free topologies on rumor dynamics. Later Chen et al. [20] proposed a refined population classification and established mean-field equations for homogeneous and heterogeneous networks.

Building on the integration of rumor propagation and the optimal control theory, scholars have explored dynamic intervention strategies along two main lines. Classical analytical approaches rely on Pontryagin's maximum principle (PMP) or Legendre spectral methods, which require solving high-dimensional adjoint equations and are sensitive to initial guesses [21–23]. Data-driven alternatives, notably multi-agent reinforcement learning (RL) and proximal policy optimization (PPO), have addressed channel uncertainties and communication delays in malware suppression [24–26], while model-based Soft Actor-Critic and meta-RL have reduced control overhead or improved sample

efficiency in sensor networks [27, 28]. Despite their differences, both lines typically overlook intervention fatigue: analytical methods assume the constant control efficiency, and RL methods rely on extensive environment rollouts and reward shaping to implicitly encode constraints, thus rendering them potentially ineffective under sustained debunking campaigns.

In recent years, physics-informed neural networks (PINNs) have provided new avenues to solve control problems in complex dynamical systems. Raissi et al. [29] embedded physical laws into the neural network loss function to efficiently solve forward and inverse problems. In epidemic control, Kim et al. [30] applied PINNs to design optimal vaccination strategies for the SIR model, thus circumventing adjoint equations; Zhong et al. [31] proposed a PINN-based model predictive control framework for real-time SIR feedback. Calafiore et al. [32] combined time-varying SIRD models with data-driven methods to support COVID-19 decision-making. However, the existing PINN control frameworks have primarily focused on infectious diseases, thus leaving their application to rumor governance largely unexplored. As a behavioral feedback mechanism, cognitive fatigue presents unique modeling challenges distinct from biological contagion: The fatigue state depends not only on the current intervention intensity but also exhibits memory and recovery characteristics, thus necessitating specialized architectures.

To address this gap, this paper proposes a framework that integrates cognitive fatigue with neural feedback control for rumor propagation governance. We introduce the SHIR-F model to treat cognitive fatigue as a system state, where the effective debunking efficiency exponentially decays with accumulated fatigue, thus capturing the diminishing returns of repeated interventions. We prove positive invariance, global existence, and uniqueness of solutions, and derive an explicit basic reproduction number that shows how fatigue levels monotonically modulate the propagation thresholds. For the control design, we develop a dual-branch neural network with a peak branch for aggressive intervention during high-risk phases and a regular branch for maintenance during stable periods, combined through fixed-weight fusion. Numerical experiments demonstrate the effectiveness of this approach in peak suppression, cost reduction, and robustness to parameter variations.Unlike black-box RL methods that learn dynamics from sampled trajectories, the proposed framework exploits the known SHIR-F structure through a differentiable simulation, thus enabling gradient-based optimization without repeated rollouts. Hard state constraints are analytically ensured via Theorem 1. The two paradigms are complementary: RL methods are well-suited to settings with unknown dynamics, whereas the present approach targets known but computationally challenging nonlinear couplings.

The remainder of this paper is structured as follows: Section 2 introduces the SHIR-F model and the optimal control formulation; Section 3 analyzes the mathematical properties; Section 4 presents the neural feedback control algorithm; Section 5 validates the method through numerical experiments; and Section 6 summarizes and discusses future directions.

## 2. The rumor propagation model

This section introduces the SHIR-F model with cognitive fatigue. We describe the state compartments and transfer rules, then establish the governing differential equations. The key innovation is treating fatigue as an endogenous state that modulates the intervention efficiency via exponential decay.

### 2.1. The state transfer rules between individuals

The SHIR-F model extends the classical SIHR framework by introducing cognitive fatigue. The population is divided into four compartments: susceptible individuals, $S(t)$, who have not yet been exposed to the rumor; hesitant individuals, $H(t)$, who have encountered the rumor but remain undecided whether to spread; spreader individuals, $I(t)$, who are actively disseminating; and recovered individuals, $R(t)$, who do not believe the rumor and may engage in debunking. Define $N$ as the constant total population, where $S(t), H(t), I(t), R(t) \geq 0$, and satisfy the following:

$$S(t) + H(t) + I(t) + R(t) = N. \tag{2.1}$$

Individuals transition between compartments through both natural processes and intervention-induced pathways. Susceptible individuals who encounter the rumor typically enter the hesitant state at a rate of $\beta(t)$, though some may directly transition to recovered through effective debunking at a rate of $\omega_S \alpha_{\text{eff}}(t)$. Hesitant individuals face three possible outcomes: becoming spreaders at a rate of $\delta$, spontaneously recovering at a rate of $\eta_H$, or being converted to recovered through intervention at a rate of $\omega_H \alpha_{\text{eff}}(t)$. Spreaders eventually cease dissemination either naturally at a rate of $\gamma$ or through intervention at a rate of $\omega_I \alpha_{\text{eff}}(t)$. The transmission rate follows $\beta(t) = \beta_{\text{base}} e^{-t/T_d}$, where $\beta_{\text{base}}$ is the initial contact rate and $T_d = 60$ is the decay time constant. This exponential decay reflects the natural attenuation of rumor spread over time. The intervention coefficients $\omega_S, \omega_H, \omega_I \in [0, 1]$ represent the relative intensity of debunking efforts applied to each compartment.

### 2.2. Dynamics of the SHIR-F model

The state transfer rules described above yield the following system of differential equations:

$$\dot{S} = -\beta(t)\frac{SI}{N} - \omega_S \alpha_{\text{eff}}(t) S, \tag{2.2}$$

$$\dot{H} = \beta(t)\frac{SI}{N} - (\delta + \eta_H) H - \omega_H \alpha_{\text{eff}}(t) H, \tag{2.3}$$

$$\dot{I} = \delta H - \gamma I - \omega_I \alpha_{\text{eff}}(t) I, \tag{2.4}$$

$$\dot{R} = \gamma I + \eta_H H + \alpha_{\text{eff}}(t)(\omega_S S + \omega_H H + \omega_I I), \tag{2.5}$$

$$\dot{F} = \eta_F u(t) - \kappa_F F. \tag{2.6}$$

Figure 1 illustrates the structure of the SHIR-F model, showing the flow of individuals between compartments and the modulation of the intervention efficiency by cognitive fatigue.

To capture the psychological weariness induced by the repeated exposure to rumor information, we introduce the cognitive fatigue variable $F(t) \geq 0$. Its dynamics are governed by $\dot{F} = \eta_F u(t) - \kappa_F F$, where the positive term $\eta_F u(t)$ represents fatigue accumulation driven by the intervention intensity $u(t) \in [0, 1]$, and the negative term $-\kappa_F F$ represents a natural recovery. Specifically, $\eta_F > 0$ is the fatigue growth coefficient, while $\kappa_F > 0$ is the fatigue recovery coefficient. This formulation aligns with the law of diminishing marginal utility in information dissemination: as the exposure to rumors increases, an individuals' sensitivity declines, manifesting as accumulated fatigue. Conversely, in the absence of new rumor stimuli, the fatigue state undergoes exponential relaxation, thereby simulating the psychological forgetting curve, where fatigue naturally subsides over time.

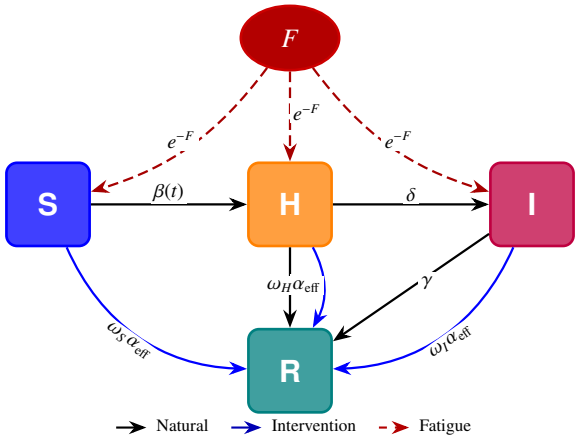


**Figure 1.** Structural diagram of the SHIR-F model. **S**: Susceptible, **H**: Hesitant, **I**: Spreader, **R**: Recovered, **F**: cognitive fatigue. Black arrows denote natural transitions; blue arrows denote intervention-induced transitions; red dashed arrows indicate fatigue modulation of debunking efficiency.

Unlike existing models that treat the intervention efficiency as an exogenous parameter, the SHIR-F model treats fatigue as an endogenous state that evolves with the history of interventions, with its dynamics driven by control inputs and regulated by a natural recovery.

The key innovation of the SHIR-F model lies in the effective debunking efficiency:

$$\alpha_{\text{eff}}(t) = \alpha_{\text{base}}(1 + u(t))e^{-F(t)}, \tag{2.7}$$

where the factor $(1 + u(t))$ captures the linear enhancement of the debunking efficiency with the intervention intensity, and the exponential decay term $e^{-F(t)}$ characterizes the diminishing marginal effect induced by fatigue.

Given the clarified dynamic role of $u(t)$, this paper formulates the intervention problem as a finite-horizon optimal control problem, aiming to strike a balance among suppressing the transmission peaks, minimizing cumulative infections, and ensuring the sustainability of interventions:

$$\min_{u(t)\in[0,1]} \int_0^T \left[a \cdot w(t)I(t) + b \cdot u^2(t) + c \cdot F^2(t)\right] \mathrm{d}t. \tag{2.8}$$

Here, $T$ is the control time domain, and $a, b, c > 0$ are weight coefficients.

To capture the time-varying marginal social benefit of infection suppression, we define a time-weight function $w(t)$ as follows:

$$w(t) = \begin{cases} 1 + \theta\frac{t}{T_1}, & 0 \le t \le T_1, \\ 1 + \theta, & T_1 < t \le T_2, \\ 1 + \theta exp(-\epsilon(t - T_2)), & t > T_2. \end{cases} \tag{2.9}$$

Here, $T_1$ denotes the time at which the infected population reaches its peak, $T_2$ denotes the end of the peak plateau period, $\theta > 0$ controls the peak weight increment, and $\epsilon > 0$ governs the decay rate of urgency in the post-peak phase. This design ensures the continuity of $w(t)$ at $T_1$ and $T_2$, and its

unimodal evolution aligns with the natural rumor propagation cycle: linearly increasing during the incubation-to-outbreak phase, remaining at its maximum during the peak plateau, and exponentially decaying as the rumor naturally subsides.

## 3. Theoretical analysis

This section establishes a mathematical theoretical framework for the SHIR-F system, thereby laying a rigorous analytical foundation for the subsequent design of control algorithms. First, we prove the positive invariance of the system within the physically feasible region and the global existence of solutions. Then, based on the next-generation matrix method, we derive an explicit expression for the basic reproduction number and analyze the modulation mechanism of the fatigue effect on the transmission threshold.

**Lemma 1** (Comparison principle)**.** *Suppose $y(t)$ satisfies the linear differential equation $\dot{y} = \eta_F - \kappa_F y$, where $\eta_F, \kappa_F > 0$, and satisfies the initial conditions $y(0) = F(0) \geq 0$. If $F(t)$ satisfies the inequality $\dot{F} \leq \eta_F - \kappa_F F$ and $F(0) = y(0)$, then $F(t) \leq y(t)$ for all $t \geq 0$.*

*Proof.* Define $z(t) = y(t) - F(t)$; then,

$$\dot{z} = \dot{y} - \dot{F} \geq (\eta_F - \kappa_F y) - (\eta_F - \kappa_F F) = -\kappa_F (y - F) = -\kappa_F z.$$

Hence, we obtain the following differential inequality: $\dot{z}(t) \geq -\kappa_F z(t)$, and $z(0) = 0$.

Following Gronwall's idea (via the integrating factor method), we get the following: $\frac{d}{dt}(z(t)e^{\kappa_F t}) \geq 0$ (i.e., $z(t)e^{\kappa_F t}$ is monotonically non-decreasing); hence, for all $t \geq 0$, $z(t)e^{\kappa_F t} \geq z(0)e^{\kappa_F \cdot 0} = 0$. Therefore, since $e^{\kappa_F t} > 0$, $z(t) \geq 0$ (i.e., $F(t) \leq y(t)$ for all $t \geq 0$). □

**Lemma 2** (Conservation of population)**.** *For any $t \geq 0$, the SHIR-F system satisfies the conservation of total population as follows:*

$$S(t) + H(t) + I(t) + R(t) = N.$$

*Proof.* The following can be directly calculated from Eqs (2.2)–(2.5):

$$\begin{aligned}\frac{d}{dt}(S + H + I + R) = &\left[-\beta(t)\frac{SI}{N} - \omega_S \alpha_{\text{eff}}(t) S\right] + \left[\beta(t)\frac{SI}{N} - (\delta + \eta_H)H - \omega_H \alpha_{\text{eff}}(t) H\right] \\ &+ \left[\delta H - \gamma I - \omega_I \alpha_{\text{eff}}(t) I\right] + \left[\gamma I + \eta_H H + \alpha_{\text{eff}}(t)(\omega_S S + \omega_H H + \omega_I I)\right] \\ = &\, 0.\end{aligned}$$

Therefore, the SHIR-F system satisfies the condition of total population conservation. □

**Theorem 1** (Positive invariance and global existence)**.** *Assume that the control input satisfies $u(t) \in [0, 1]$ $(\forall t \geq 0)$, and the model parameters satisfy the following:*

$$\beta_{\text{base}}, \delta, \gamma, \eta_H, \alpha_{\text{base}}, \eta_F \geq 0, \quad \kappa_F > 0, \quad \omega_S, \omega_H, \omega_I \in [0, 1].$$

*If the initial conditions satisfy, $S(0), H(0), I(0), R(0), F(0) \geq 0$, $S(0) + H(0) + I(0) + R(0) = N$, $F(0) \leq \frac{\eta_F}{\kappa_F}$, then the initial value problem (2.2)–(2.6) admits a unique global solution $(S(t), H(t), I(t), R(t), F(t))$, and for all $t \in [0, +\infty)$, the following properties hold: non-negativity $S(t), H(t), I(t), R(t), F(t) \geq 0$; and boundedness of fatigue $0 \leq F(t) \leq \eta_F/\kappa_F$.*

*Proof.* The state space is defined as follows:

$$\Omega := \left\{ (S, H, I, R, F) \in \mathbb{R}^5_{\geq 0} : S + H + I + R = N,\ 0 \leq F \leq \frac{\eta_F}{\kappa_F} \right\}.$$

Based on Eqs (2.2)–(2.5), and when each state variable reaches the zero boundary,

$$\begin{aligned}
&S(t) = 0 \Longrightarrow \dot{S} = 0 \geq 0,\\
&H(t) = 0 \Longrightarrow \dot{H} = \beta(t)\frac{SI}{N} \geq 0,\\
&I(t) = 0 \Longrightarrow \dot{I} = \delta H \geq 0,\\
&R(t) = 0 \Longrightarrow \dot{R} = \gamma I + \eta_H H + \alpha_{\text{eff}}(t)(\omega_S S + \omega_H H + \omega_I I) \geq 0,\\
&F(t) = 0 \Longrightarrow \dot{F} = \eta_F u(t) \geq 0.
\end{aligned}$$

It can be seen that the system vector field always points inward or tangentially along the boundary of the non-negative orthant. By Nagumo's positive invariance theorem, $\Omega$ is a positively invariant set of the system, and $S(t), H(t), I(t), R(t), F(t) \geq 0$ hold for all $t \geq 0$.

For $F(t)$, by Lemma 1 and $\dot{F} \leq \eta_F - \kappa_F F$, we obtain $F(t) \leq \eta_F/\kappa_F$. The global existence of solutions is guaranteed by the boundedness of the compact set and the Picard–Lindelöf theorem. □

The basic reproduction number $\mathcal{R}_0$ is a core threshold parameter in epidemic and rumor propagation models, thus representing the average number of new individuals infected by a typical infectious individual during the entire infectious period in a fully susceptible population. This section derives the basic reproduction number for the SHIR-F system based on the next-generation matrix method, and analyzes the modulation mechanism of cognitive fatigue on the propagation threshold.

**Proposition 1** (The existence of the rumor-free equilibrium)**.** *Assume the system is in an intervention-free state and fatigue is in a steady state (i.e., $u(t) \equiv 0$). Then, System* (2.2)–(2.6) *has a rumor-free equilibrium $E_0 = (N, 0, 0, 0, 0)$.*

*Proof.* Set $\dot{F} = 0$ and $u = 0$; from Eq (2.6), we obtain $F^* = 0$. Let $H = I = 0$; population conservation (2.1) yields $S + R = N$. When $I = 0$, Eq (2.2) reduces to $\dot{S} = -\omega_S \alpha_{\text{base}} S$.

When $\dot{S} = 0$, if $S \neq 0$, then necessarily $\omega_S = 0$ (in the absence of intervention, susceptible individuals do not spontaneously transition to fact-checkers), thus yielding the initial rumor-free equilibrium of the system $E_0 = (N, 0, 0, 0, 0)$ (there are no spreaders in the system, and the system is in an initial equilibrium state).

Note: If $S = 0$, then the system degenerates into an absorbing state $(0, 0, 0, N)$, which will not be further discussed in this paper. □

Before analyzing the effect of cognitive fatigue, we first consider the baseline scenario where fatigue has not yet accumulated ($F = 0$) and no intervention is applied ($u = 0$). In this case, the basic reproduction number $\mathcal{R}_0$ at the rumor-free equilibrium $E_0$ is defined as follows.

**Proposition 2** (Basic reproduction number and local stability)**.** *At the rumor-free equilibrium $E_0$, the basic reproduction number of the SHIR-F system is as follows:*

$$\mathcal{R}_0 = \frac{\beta_{\text{base}}\delta}{(\gamma + \omega_I \alpha_{\text{base}})(\delta + \eta_H + \omega_H \alpha_{\text{base}})}. \tag{3.1}$$

*When $\mathcal{R}_0 < 1$, $E_0$ is locally asymptotically stable and the rumor eventually dies out; when $\mathcal{R}_0 > 1$, $E_0$ is unstable and the rumor can spread persistently in the system.*

*Proof.* We employ the next-generation matrix method proposed by van den Driessche and Watmough [33], where the system states are partitioned into uninfected compartments $\mathbf{x} = (S, R, F)^T$ and infected compartments $\mathbf{y} = (H, I)^T$.

Linearizing near $E_0$, the new infection terms and transition terms are given by the following:

$$\mathcal{F}(\mathbf{y}) = \begin{pmatrix} \beta_{\text{base}} I \\ 0 \end{pmatrix}, \quad \mathcal{V}(\mathbf{y}) = \begin{pmatrix} (\delta + \eta_H + \omega_H \alpha_{\text{base}}) H \\ (\gamma + \omega_I \alpha_{\text{base}}) I - \delta H \end{pmatrix},$$

respectively.

The corresponding Jacobian matrices are as follows:

$$F = \begin{pmatrix} 0 & \beta_{\text{base}} \\ 0 & 0 \end{pmatrix}, \quad V = \begin{pmatrix} \delta + \eta_H + \omega_H \alpha_{\text{base}} & 0 \\ -\delta & \gamma + \omega_I \alpha_{\text{base}} \end{pmatrix}.$$

Calculate the inverse of matrix $V$ as follows:

$$V^{-1} = \frac{1}{(\delta + \eta_H + \omega_H \alpha_{\text{base}})(\gamma + \omega_I \alpha_{\text{base}})} \begin{pmatrix} \gamma + \omega_I \alpha_{\text{base}} & 0 \\ \delta & \delta + \eta_H + \omega_H \alpha_{\text{base}} \end{pmatrix}.$$

The next-generation matrix is given by the following:

$$FV^{-1} = \frac{1}{(\delta + \eta_H + \omega_H \alpha_{\text{base}})(\gamma + \omega_I \alpha_{\text{base}})} \begin{pmatrix} \beta_{\text{base}} \delta & \beta_{\text{base}} (\delta + \eta_H + \omega_H \alpha_{\text{base}}) \\ 0 & 0 \end{pmatrix}.$$

The eigenvalues of the Jacobian matrix are as follows: $\lambda_1 = \frac{\beta_{\text{base}} \delta}{(\delta + \eta_H + \omega_H \alpha_{\text{base}})(\gamma + \omega_I \alpha_{\text{base}})}$ and $\lambda_2 = 0$. The spectral radius is $\rho(FV^{-1}) = \max\{|\lambda_1|, |\lambda_2|\} = \lambda_1$, thus yielding (3.1).

Next, we analyze the stability at $\mathcal{R}_0$. The characteristic polynomial of the infected subsystem is as follows

$$\det(\lambda I - (F - V)) = \lambda^2 + (A + B)\lambda + AB - \beta_{\text{base}} \delta = 0,$$

where $A = \delta + \eta_H + \omega_H \alpha_{\text{base}}$,$B = \gamma + \omega_I \alpha_{\text{base}}$. According to the Routh–Hurwitz criterion, when $AB - \beta_{\text{base}} \delta > 0$ and $A + B > 0$, all eigenvalues have negative real parts. Noting that $AB(1 - \mathcal{R}_0) = AB - \beta_{\text{base}} \delta$, the following hold: if $\mathcal{R}_0 < 1$, then $E_0$ is locally asymptotically stable; and if $\mathcal{R}_0 > 1$, there exists an eigenvalue with positive real part, and $E_0$ is unstable. □

When the fatigue level $F(t)$ increases, the effective debunking efficiency $\alpha_{\text{eff}}(t)$ decreases, thus leading to an increase in the effective reproduction number. The time-varying reproduction number $\mathcal{R}(t)$ serves as a more general extension of the basic reproduction number $\mathcal{R}_0$ by incorporating the dynamic fatigue effect. In fact, when $F(0) = 0$ and $u(0) = 0$, we have $\mathcal{R}(0) = \mathcal{R}_0$.

**Theorem 2** (Modulation effect of fatigue on the reproduction number)**.** *Considering the dynamic effect of the fatigue variable $F(t) > 0$, the time-varying reproduction number is as follows:*

$$\mathcal{R}(t) = \frac{\beta_{\text{base}} \delta}{(\gamma + \omega_I \alpha_{\text{eff}}(t))(\delta + \eta_H + \omega_H \alpha_{\text{eff}}(t))}. \tag{3.2}$$

*$\mathcal{R}(t)$ is strictly monotonically increasing with respect to $F(t)$ and satisfies the boundedness $\mathcal{R}_{\min} \leq \mathcal{R}(t) \leq \mathcal{R}_{\max}$.*

*Proof.* Define the following function:

$$f(\alpha) = \frac{1}{(\delta + \eta_H + \omega_H\alpha)(\gamma + \omega_I\alpha)}, \quad \alpha \geq 0.$$

Compute its derivative as follows:

$$\begin{aligned} f'(\alpha) &= -\frac{\omega_H(\gamma + \omega_I\alpha) + \omega_I(\delta + \eta_H + \omega_H\alpha)}{[(\delta + \eta_H + \omega_H\alpha)(\gamma + \omega_I\alpha)]^2} \\ &= -\frac{\omega_H\gamma + \omega_I(\delta + \eta_H) + 2\omega_H\omega_I\alpha}{[(\delta + \eta_H + \omega_H\alpha)(\gamma + \omega_I\alpha)]^2}. \end{aligned}$$

Since $\omega_H, \omega_I > 0$ and $\gamma, \delta, \eta_H \geq 0$ and $\alpha \geq 0$, we have $f'(\alpha) < 0$. Therefore, $f(\alpha)$ is strictly decreasing with respect to $\alpha$. Note that the time-varying reproduction number can be expressed as $\mathcal{R}(t) = \beta_{\text{base}}\delta \cdot f(\alpha_{\text{eff}}(t))$. From the definition of the effective debunking efficiency (2.7), $\alpha_{\text{eff}}(t) = \alpha_{\text{base}}(1 + u(t))e^{-F(t)}$, when $u(t) \in [0, 1]$ is held fixed, $\alpha_{\text{eff}}(t)$ is strictly decreasing with respect to $F(t)$. Since $f$ is strictly decreasing, the composite function $\mathcal{R}(t) = \beta_{\text{base}}\delta \cdot f(\alpha_{\text{eff}}(t))$ is strictly increasing with respect to $F(t)$. Boundedness proof: By Theorem 1, $0 \leq F(t) \leq \eta_F/\kappa_F$ and $u(t) \in [0, 1]$, we have

$$\alpha_{\text{base}}e^{-\eta_F/\kappa_F} \leq \alpha_{\text{eff}}(t) \leq 2\alpha_{\text{base}}.$$

Since $f(\alpha)$ is strictly decreasing,

$$f(2\alpha_{\text{base}}) \leq f(\alpha_{\text{eff}}(t)) \leq f(\alpha_{\text{base}}e^{-\eta_F/\kappa_F}).$$

Therefore,

$$\mathcal{R}_{\min} = \frac{\beta_{\text{base}}\delta}{(\gamma + 2\omega_I\alpha_{\text{base}})(\delta + \eta_H + 2\omega_H\alpha_{\text{base}})},$$

$$\mathcal{R}_{\max} = \frac{\beta_{\text{base}}\delta}{(\gamma + \omega_I\alpha_{\text{base}}e^{-\eta_F/\kappa_F})(\delta + \eta_H + \omega_H\alpha_{\text{base}}e^{-\eta_F/\kappa_F})},$$

where

$$\lim_{\frac{\eta_F}{\kappa_F} \to \infty} \mathcal{R}_{\max} = \frac{\beta_{\text{base}}\delta}{\gamma(\delta + \eta_H)}.$$

□

Theorem 2 reveals the core mechanism of cognitive fatigue: fatigue not only reduces the effectiveness of rumor refutation but also amplifies the risk of rumor propagation through a monotonically increasing reproduction number function. This fatigue-propagation positive feedback mechanism implies that, without timely adjustment of intervention strategies, the system may fall into a vicious cycle of high fatigue, low efficiency, and high transmission. The value of neural feedback control lies in dynamically regulating $u(t)$ through real-time state observation, thereby seeking an optimal balance between fatigue accumulation and transmission suppression.

*Existence of optimal control*

**Proposition.** The cost functional $J(u)$ for the SHIR-F system admits at least one optimal control $u^*(t) \in L^2([0,T],[0,1])$.

*Proof.* The cost is as follows:

$$J(u) = \int_0^T aw(t)I(t;u) + bu(t)^2 + cF(t;u)^2 \, dt. \tag{3.3}$$

The terms $bu(t)^2$ and $cF(t;u)^2$ (where $F$ is affine in $u$ via the linear dynamics $\dot{F} = \eta_F u - \kappa_F F$) are strictly convex. The infection cost is nonnegative.

$J(u)$ is coercive on $L^2([0,T])$ since $J(u) \geq b\|u\|_{L^2}^2$. Furthermore, the solution map $u \mapsto (I(t;u), F(t;u))$ is continuous from $L^2([0,T])$ to $C([0,T])$ under the Lipschitz continuity of the SHIR-F dynamics, thus implying that $J$ is weakly lower semicontinuous. Hence, a minimizer exists. □

Although a full analytic proof of strict convexity is obstructed by nonlinear ordinary differential equation (ODE) coupling in the infection dynamics, the structural strict convexity of control and fatigue terms suggests uniqueness. This theoretical prediction will be numerically validated in Section 5.

## 4. Neural feedback control algorithm

This section presents an end-to-end optimal control framework using deep neural networks. Traditional indirect methods based on PMP require solving high-dimensional adjoint equations and are sensitive to initial guesses. The proposed approach directly optimizes the control policy parameters through differentiable dynamic simulation, using automatic differentiation to efficiently compute gradients and avoid two-point boundary value problems.

A dual-branch fully connected neural network implements the state-feedback control law $u_\theta : \mathbb{R}^5 \to [0,1]$. The network maps the current system state $x = (S, H, I, R, F)$ to the control input $u$, with functional decoupling achieved through branch specialization. The input layer receives a 5-dimensional state vector. The peak suppression branch employs a 2-layer fully connected network, thereby focusing on aggressive intervention during high-risk phases. The first layer captures nonlinear relationships in the state space, followed by feature compression in the second layer to output control decisions. The regular branch adopts a symmetric 2-layer network responsible for maintaining control during stable periods to avoid fatigue accumulation from excessive interventions. The fusion layer combines outputs from both branches with fixed weights $w_p$ and $w_r$, and the result is constrained by a Sigmoid function as follows:

$$u_\theta(x) = \sigma\big(w_p\, u_p + w_r\, u_r\big) \in (0,1), \tag{4.1}$$

where $w_p + w_r = 1$ are constant fusion weights. In implementation, $w_p = 0.7$ and $w_r = 0.3$ emphasize the peak suppression branch while retaining the regulation effect of the regular branch. Fixed-weight fusion avoids gradient oscillations from dynamic weights, thus ensuring numerical stability. Constant gradient proportions with respect to branch parameters avoid additional nonlinearity and instability.

The continuous-time optimal control problem (2.8) is discretized into a finite-dimensional optimization problem. The time interval $[0,T]$ is uniformly discretized into $N_T = T/\Delta t$ time steps, with $t_n = n\Delta t$. The fourth-order Runge–Kutta method advances the system dynamics as follows:

$$x_{n+1} = x_n + \frac{\Delta t}{6}(k_1 + 2k_2 + 2k_3 + k_4), \tag{4.2}$$

where $k_1, k_2, k_3, k_4$ represent the RK4 increment. The discretized optimization objective is as follows:

$$\min_{\theta} J(\theta) = \sum_{n=0}^{N_T-1} \left[a \cdot w(t_n) \cdot I_n + b \cdot u_n^2 + c \cdot F_n^2\right] \Delta t. \tag{4.3}$$

Figure 2 illustrates the dual-branch neurofeedback optimal control framework. The complete training procedure is summarized in Algorithm 1, which implements gradient-based optimization with stability mechanisms, including gradient clipping and early stopping.

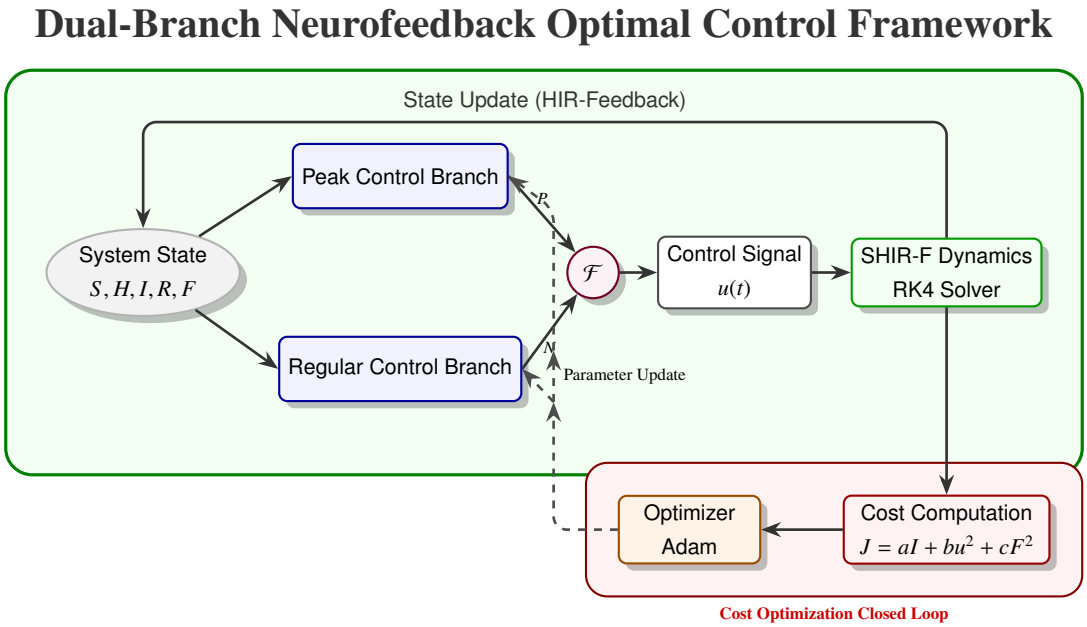


**Figure 2.** Dual-Branch neurofeedback optimal control framework.

Algorithm 1 summarizes the training procedure, which uses the Adam optimizer with gradient clipping, learning rate scheduling, and early stopping to ensure numerical stability.

**Algorithm 1** Optimal control algorithm for SHIR-F based on dual-branch neural network.

**Input:** Initial condition $x_0 = (S_0, H_0, I_0, R_0, F_0)$; System parameters; Time configuration $[0, T]$, $\Delta t$; Cost weights $a, b, c$ and Stage weights; Network hyperparameters
**Output:** Optimal policy parameters $\theta^*$; Closed-loop trajectory
Initialize network parameters $\theta^{(0)}$, $J_{\text{best}} \leftarrow +\infty$, $p \leftarrow 0$
**for** $e = 1$ to $E_{\max}$ **do**
    $x \leftarrow x_0$, $J \leftarrow 0$
    **for** $n = 0$ to $N_T - 1$ **do**
        $u_n \leftarrow \sigma(w_p\, u_p(x_n) + w_r\, u_r(x_n))$
        $x_{n+1} \leftarrow \text{RK4}(x_n, u_n, \Delta t)$
        $x_{n+1} \leftarrow \Pi_\Omega(x_{n+1})$
        $J \leftarrow J + [aw(t_n)I_n + bu_n^2 + cF_n^2]\Delta t$
    **end for**
    $\nabla_\theta J \leftarrow \text{Backprop}(J, \theta^{(e-1)})$
    $\nabla_\theta J \leftarrow \text{Clip}(\nabla_\theta J, 1.0)$
    $\theta^{(e)} \leftarrow \text{Adam}(\theta^{(e-1)}, \nabla_\theta J, \eta)$
    $\eta \leftarrow \text{CosineAnnealing}(e)$
    **if** $J$ no further improvement **then**
        $p \leftarrow p + 1$
    **end if**
    **if** $p \geq P$ **then**
        **break**
    **end if**
**end for**
**return** $\theta^*$

## 5. Numerical experiments and results analysis

In this section, we conduct experiments using the proposed neural feedback controller algorithm, and its effectiveness is verified by comparison with PMP .

### *5.1. Numerical configuration and parameter settings*

Numerical experiments are conducted under a unified parameter configuration. The control horizon is $[0, T]$ with $T = 60$ time units, discretized into 300 steps ($\Delta t = 0.2$). Model parameters and initial conditions are summarized in Table 1. The uncontrolled system exhibits a pronounced infection peak, thus serving as a clear baseline for comparison.

**Table 1.** SHIR-F model parameters and initial conditions.

| Category | Parameter | Value |
|---|---|---|
| Population | $N$ | 1000 |
| Initial state | $(S_0, H_0, I_0, R_0)$ | $(850, 100, 50, 0)$ |
| Initial fatigue | $F(0)$ | 0 |
| Transmission | $\beta_{\text{base}}$ | 0.50 |
| | $T_d$ (decay time) | 60 |
| | $\delta, \gamma$ | 0.40, 0.05 |
| | $\eta_H$ | 0.05 |
| Intervention | $\alpha_{\text{base}}$ | 0.10 |
| | $(\omega_S, \omega_H, \omega_I)$ | $(0.2, 0.3, 0.5)$ |
| | $\eta_F, \kappa_F$ | 0.20, 2.0 |
| Objective | $(a, b, c)$ | $(3.0, 0.05, 0.20)$ |
| Time weight | $(\theta, \epsilon, T_2)$ | $(9.0, 0.1, 30.0)$ |
| Time | $T, \Delta t$ | 60, 0.2 |

The neural controller employs a dual-branch architecture with fixed fusion weights. For reference, the training hyperparameters and the PMP configuration are provided in Table 2.

**Table 2.** Neural controller and PMP configuration.

| | |
|---|---|
| Network architecture | 5→64→32→1 (per branch) |
| Fusion weights | $w_p = 0.7$, $w_r = 0.3$ |
| Total parameters | $\approx 8 \times 10^3$ |
| Optimizer | Adam |
| Learning rate | $1.5 \times 10^{-3} \rightarrow 10^{-4}$ (cosine) |
| Gradient clipping | Max norm 1.0 |
| Early stopping | 100 epochs, threshold $10^{-4}$ |
| PMP optimizer | L-BFGS-B |
| PMP segments | 30 |
| PMP max iterations | 200 |

A single forward pass requires $O(N_T \cdot P)$ operations, where $P \approx 8 \times 10^3$ is the number of trainable parameters. Training was performed on an NVIDIA GeForce GTX 1650 Ti GPU, with typical convergence within 200 epochs.

### *5.2. Temporal dynamics and optimality validation*

Figure 3 shows the infection dynamics under neurofeedback regulation. The infection peak is reduced from 248.00 to 155.25 (37.4% suppression); the peak time decreases from 13.20 to 9.80 time units. This indicates that the control strategy redistributes the transmission intensity over time by reshaping the transient dynamics, thus reserving a critical response window for subsequent

interventions.

To validate the optimality, we compare with a baseline obtained via direct numerical optimization (L-BFGS-B, 30 piecewise-constant segments). As summarized in Table 3, both methods converge to essentially the same trajectory with negligible differences ($< 0.01\%$), thus confirming that the neural controller successfully learns the optimal policy. However, the two methods differ in the control architecture: the baseline yields a pre-computed open-loop trajectory $u^*(t)$, whereas the neural controller implements a closed-loop state feedback $u_\theta(x(t))$ that adjusts the intervention based on real-time observations of $(S, H, I, R, F)$. This distinction is critical when the model parameters deviate from nominal values—the open-loop solution cannot compensate for such deviations, whereas the closed-loop controller naturally adapts without re-optimization.

**Table 3.** Comprehensive performance comparison across three scenarios.

| Metric | Uncontrolled | PMP | Neural | Suppression (%) | PMP-Neural Diff (%) |
|---|---|---|---|---|---|
| Peak infection | 248.00 | 155.25 | 155.25 | 37.40 | $< 0.01$ |
| Peak time | 13.20 | 9.80 | 9.80 | – | – |
| Total cost | 155605.04 | 79686.96 | 79686.96 | 48.79 | $< 0.01$ |
| I-integral | 6535.21 | 3456.79 | 3456.79 | 47.11 | $< 0.01$ |
| Clearance rate | – | 87.9% | 87.9% | – | $< 0.01$ |

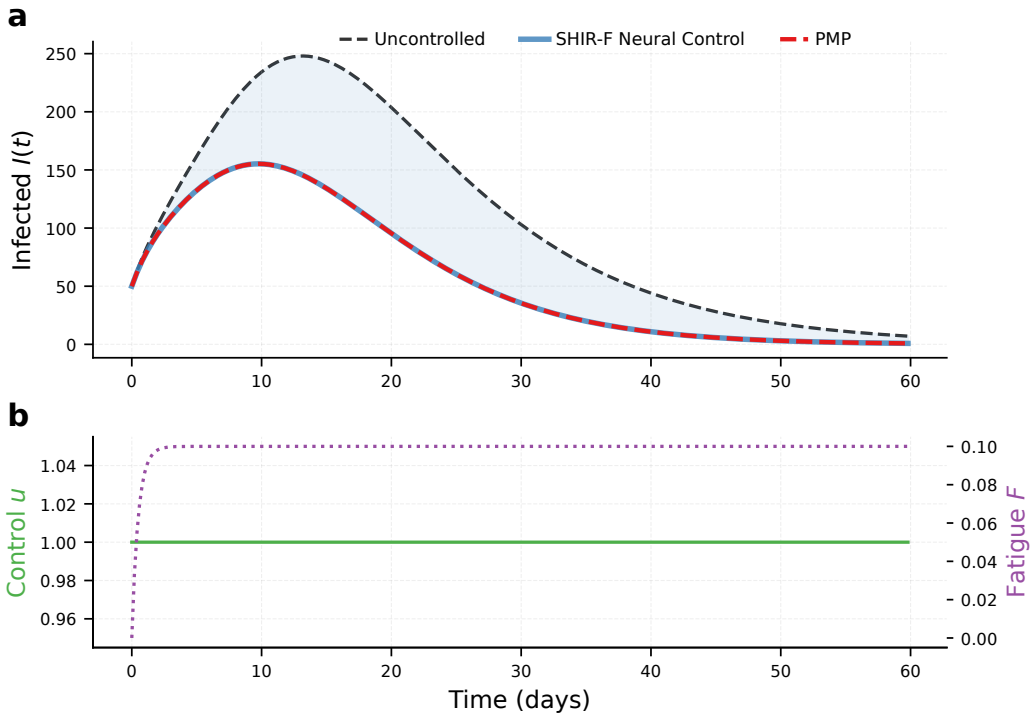


**Figure 3.** Infection dynamics and control strategy. (Top) Three scenarios: uncontrolled (peak 248.00), PMP (peak 155.25), neural (peak 155.25). Shaded area indicates infections averted. (Bottom) Control intensity $u(t)$ and fatigue $F(t)$.

### 5.3. Control-fatigue coupling and phase plane analysis

The control intensity $u(t)$ remains near its upper bound throughout the control horizon. Fatigue $F(t)$ increases during the initial intervention phase and remains bounded thereafter. This boundedness ensures $\alpha_{\text{eff}}(t) > 0$, thus preventing the efficiency collapse from excessive fatigue accumulation.

Figure 4 shows the S-I phase plane trajectories. The closed-loop control steers the system from $(S_0, I_0) = (850, 50)$ toward the low-infection region, with peak infection reduced from approximately 250 to 155. The controlled trajectory remains below the uncontrolled path throughout. The trajectories remain bounded within the physically feasible region, which is consistent with Theorem 1.

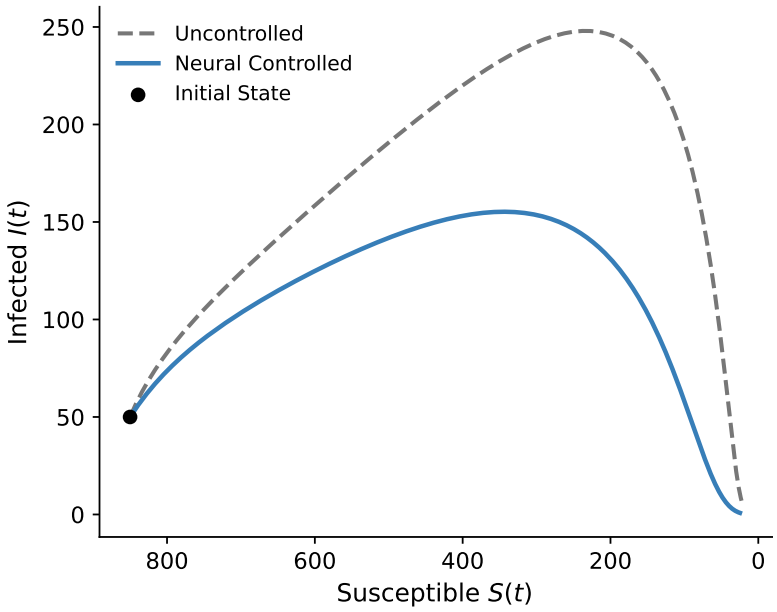


**Figure 4.** S-I phase plane trajectories. Blue solid: controlled; red dashed: uncontrolled; arrows: time direction. The control strategy steers the system toward the low-infection region.

### 5.4. Robustness

To assess the practical applicability, the neural controller is evaluated under ±10% perturbations in core parameters $(\beta, \delta, \gamma, \alpha)$ without retraining. Table 4 summarizes the results: Peak infection ranges from 142.03 ($\beta - 10\%$) to 170.41 ($\alpha - 10\%$), with suppression rates between 31.29% and 42.74%.

**Table 4.** Robustness under ±10% parameter perturbations.

| **Metric** | $\beta$ | $\delta$ | $\gamma$ | $\alpha$ |
|---|---|---|---|---|
| +10%: $I_{\max}$ | 168.57 | 163.41 | 150.24 | 142.41 |
| +10%: Supp. (%) | 32.03 | 34.19 | 39.38 | 42.58 |
| Baseline | | 155.25 / 37.40% | | |
| −10%: $I_{\max}$ | 142.03 | 146.28 | 160.55 | 170.41 |
| −10%: Supp. (%) | 42.74 | 41.02 | 35.26 | 31.29 |

The transmission rate $\beta$ and debunking efficiency $\alpha$ exhibit the highest sensitivity, while the recovery rate $\gamma$ shows relatively mild effects. All perturbed scenarios preserve a unimodal trajectory structure and system stability.

Figure 5 shows infection and fatigue trajectories under ±10% parameter perturbations. All scenarios maintain single-peak dynamics with an effective terminal clearance. Fatigue remains bounded and nearly identical across perturbations. The transmission rate $\beta$ and debunking efficiency $\alpha$ exhibit higher sensitivities than $\gamma$ and $\delta$, which is consistent with the SHIR-F model structure.

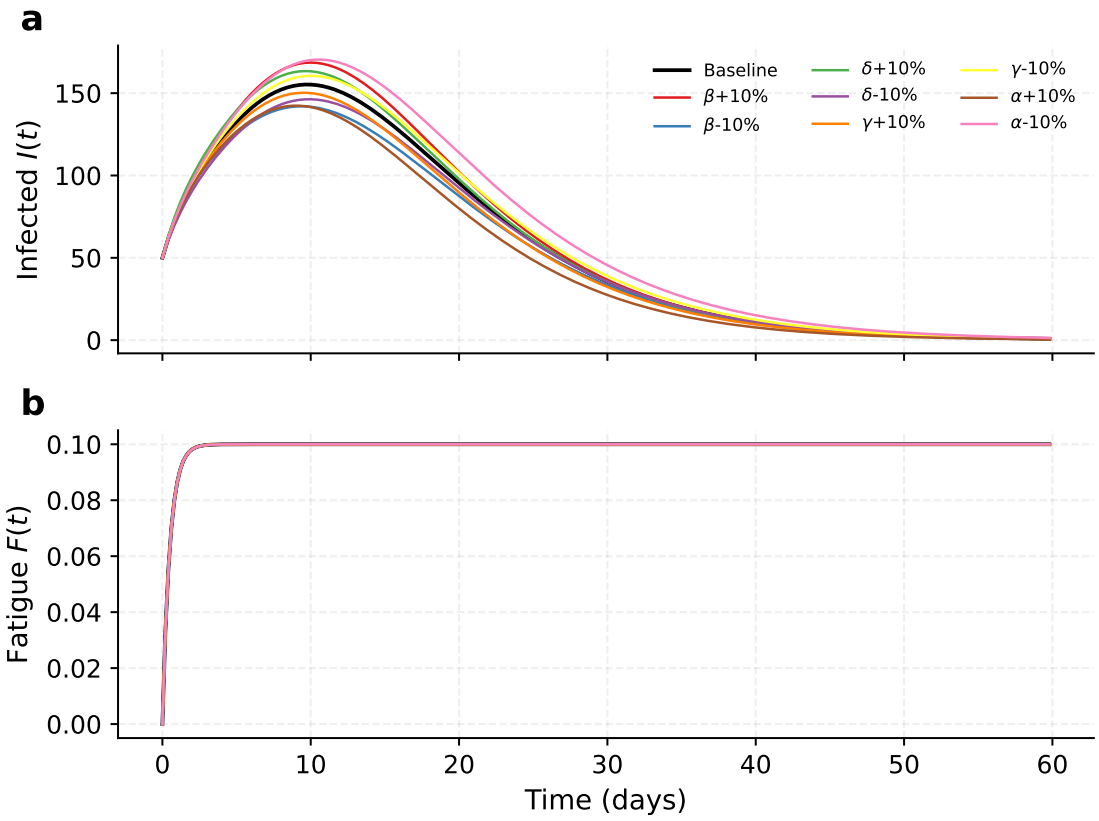


**Figure 5.** Robustness analysis under ±10% parameter perturbations. (a) Infection trajectories $I(t)$; (b) Fatigue evolution $F(t)$. All scenarios preserve unimodal structure and effective clearance.

### *5.5. Analysis of fusion weight invariance*

Table 3 shows neural and PMP convergences to identical optimal trajectories, thus numerically validating the uniqueness predicted in Section 3. Now, we explain the observed invariance to fusion weights $(w_p, w_r)$.

#### 5.5.1. Heuristic argument for fusion weight invariance

The dual-branch controller is as follows:

$$u(x) = \sigma(w_p f_p(x) + w_r f_r(x)), \quad x = (S, H, I, R, F, t),$$

with $w_p + w_r = 1$, $w_p, w_r \geq 0$, where $f_p$ and $f_r$ share identical architectures and initialization.

For any valid $(w_p, w_r)$, the representable set is as follows:

$$\mathcal{U}_{w_p,w_r} = \{\sigma(w_p f_p + w_r f_r) \mid f_p, f_r \in \mathcal{F}\},$$

where $\mathcal{F}$ is the function class of a single branch. Although these sets slightly differ for finite-width networks, they possess nearly equivalent expressive powers. The universal approximation theorem suggests that networks with a sufficient capacity can approximate continuous functions on compact domains arbitrarily well. With approximately $8 \times 10^3$ parameters, both branches possess comparable expressive capacities.

Training minimizes $J(u)$ over search spaces of essentially identical approximation capacities. Assuming the uniqueness of $u^*$ (validated numerically above), gradient-based optimization converges to essentially the same trajectory regardless of the specific fusion weights chosen. Different $(w_p, w_r)$ mainly alter the optimization path in the parameter space rather than the attainable controls at convergence. This explains the observed approximate invariance, despite differing internal representations due to non-convexity of the parameter space.

#### 5.5.2. Theoretical and practical implications

The consistent performance across fusion weights follows from the uniqueness of $u^*$ and the stable representational capacity of the dual-branch architecture under different convex combinations. This unifies the close PMP-neural agreement with fusion-weight invariance as two manifestations of the same underlying property.

In this convex-in-control-cost setting, a single well-designed network achieves a performance comparable to the dual-branch design. Nevertheless, multi-branch or ensemble architectures remain advantageous for non-convex problems, complex optimal policies, or when greater robustness to initialization and training noise is needed.

## 6. Conclusions

This paper proposed a novel SHIR-F rumor propagation model that incorporates a cognitive fatigue state variable, $F(t)$, and an exponentially decaying debunking efficiency, $\alpha_{\text{eff}}(t) = \alpha_{\text{base}}(1 + u(t))e^{-F(t)}$, to precisely characterize psychological adaptation and information desensitization effects during long-term interventions. Based on this model, a dual-branch neural network end-to-end optimal control framework was designed, which utilizes a time-weighted cost functional to guide the controller in concentrating resources during high-risk phases, thus achieving effective infection peak suppression and transient dynamics reshaping.

Numerical experiments demonstrated that the proposed strategy achieves a 37.4% infection peak suppression and a 48.8% cost reduction compared to the uncontrolled baseline. The neural controller converges to essentially the same trajectory as the PMP (difference $< 0.01\%$), thus confirming a near-optimal performance while providing a closed-loop feedback capability. Under $\pm 10\%$ parameter perturbations, peak suppression rates range from 31.29% to 42.74% (mean 37.10%, std 3.89%), with all scenarios preserving unimodal dynamics and an effective terminal clearance, thus confirming structural robustness.

This work makes contributions to both theory and practice. The SHIR-F model expands traditional rumor propagation frameworks by formalizing intervention fatigue as a controllable nonlinear feedback mechanism. For practical deployment, the control framework can offer quantitative decision support for fact-checking on social platforms and crisis communication strategy design, particularly in scenarios that require balance between short-term suppression effects and long-term sustainability.

This work has several limitations. The current model assumes homogeneous mixing, which overlooks heterogeneous contact patterns and demographic differences in fatigue sensitivity across platforms such as Weibo or Twitter. Extensions to networked formulations would address this constraint. The neural control policy, while effective, operates as a black-box function and may face challenges in policy-making contexts that require interpretability. Moreover, the method relies on known SHIR-F dynamics; the performance would degrade if the propagation mechanisms abruptly change without online adaptation.

Future work will explore several directions. The model can be extended to networked settings to investigate the scalability and topological heterogeneity. Stochastic perturbations may enhance the robustness under real-world uncertainties. Additionally, the framework could address multi-source rumor competition with multi-channel interventions. Integrating real social media data for parameter identification would further strengthen the practical applicability.

## Author contributions

Xiaoyu Maio: Model analysis and modification; Haoran Song: Writing-original draft and software; Lipu Zhang: Supervisor. All authors have read and approved the final version of the manuscript for publication.

## Use of Generative-AI tools declaration

No generative artificial intelligence tools have been used throughout the research.

## Acknowledgments

This work was supported by Zhejiang Engineering Research Center of Intelligent Media and the Young Faculty Development Program of Communication University of Zhejiang. The relevant source code and experimental data have been publicly released on the GitHub platform, accessible at: https://github.com/locustzhang/Neural-Feedback-Control-of-Rumor-Spreading-with-Cognitive-Fatigue.

## Conflict of interest

The authors declare there are no conflicts of interest.

## References

1. D. J. Daley, D. G. Kendall, Stochastic rumours, *IMA J. Appl. Math.*, **1** (1965), 42–55. https://doi.org/10.1093/imamat/1.1.42

2. D. P. Maki, M. Thompson, *Mathematical models and applications: with emphasis on the social, life, and management sciences*, Englewood Cliffs: Prentice-Hall, 1973.
3. D. J. Daley, J. Gani, Rumours: modelling spread and its cessation, In: *Epidemic modelling: an introduction*, Cambridge Studies in Mathematical Biology, Cambridge University Press, 1999, 133–153.
4. D. H. Zanette, Dynamics of rumor propagation on small-world networks, *Phys. Rev. E*, **65** (2002), 041908. https://doi.org/10.1103/PhysRevE.65.041908
5. Y. Moreno, M. Nekovee, A. F. Pacheco, Dynamics of rumor spreading in complex networks, *Phys. Rev. E*, **69** (2004), 066130. https://doi.org/10.1103/PhysRevE.69.066130
6. M. Nekovee, Y. Moreno, G. Bianconi, M. Marsili, Theory of rumour spreading in complex social networks, *Phys. A*, **374** (2007), 457–470. https://doi.org/10.1016/j.physa.2006.07.017
7. L. Zhao, H. Cui, X. Qiu, X. Wang, J. Wang, SIR rumor spreading model in the new media age, *Phys. A*, **392** (2013), 995–1003. https://doi.org/10.1016/j.physa.2012.09.030
8. Y. Zan, J. Wu, P. Li, Q. Yu, SICR rumor spreading model in complex networks: counterattack and self-resistance, *Phys. A*, **405** (2014), 159–170. https://doi.org/10.1016/j.physa.2014.03.021
9. S. Ahmed, M. E. Rasul, Examining the association between social media fatigue, cognitive ability, narcissism and misinformation sharing: cross-national evidence from eight countries, *Sci. Rep.*, **13** (2023), 1541614. https://doi.org/10.1038/s41598-023-42614-z
10. Y. Hwang, J. So, S. H. Jeong, Does COVID-19 message fatigue lead to misinformation acceptance? An extension of the risk information seeking and processing model, *Health Commun.*, **38** (2023), 2742–2749. https://doi.org/10.1080/10410236.2022.2111636
11. A. K. M. N. Islam, S. Laato, S. Talukder, E. Sutinen, Misinformation sharing and social media fatigue during COVID-19: an affordance and cognitive load perspective, *Technol. Forecast. Soc. Change*, **159** (2020), 120201. https://doi.org/10.1016/j.techfore.2020.120201
12. E. C. Tandoc, H. K. Kim, Avoiding real news, believing in fake news? Investigating pathways from information overload to misbelief, *Journalism*, **24** (2023), 1174–1192. https://doi.org/10.1177/14648849221090744
13. O. D. Apuke, B. Omar, E. A. Tunca, C. V. Gever, Information overload and misinformation sharing behaviour of social media users: testing the moderating role of cognitive ability, *J. Inf. Sci.*, **50** (2024), 1371–1381. https://doi.org/10.1177/01655515221121942
14. L. Zhao, J. Wang, Y. Chen, Q. Wang, J. Cheng, H. Cui, SIHR rumor spreading model in social networks, *Phys. A*, **391** (2012), 2444–2453. https://doi.org/10.1016/j.physa.2011.12.008
15. H. Zhu, J. Ma, Analysis of SHIR rumor propagation in random heterogeneous networks with dynamic friendships, *Phys. A*, **513** (2019), 257–271. https://doi.org/10.1016/j.physa.2018.09.015
16. X. Chen, N. Wang, Rumor spreading model considering rumor credibility, correlation and crowd classification based on personality, *Sci. Rep.*, **10** (2020), 5887. https://doi.org/10.1038/s41598-020-62585-9
17. W. Liu, J. Wang, Y. Ouyang, Rumor transmission in online social networks under Nash equilibrium of a psychological decision game, *Netw. Spat. Econ.*, **22** (2022), 831–854. https://doi.org/10.1007/s11067-022-09574-9

18. J. Gu, W. Li, X. Cai, The effect of the forget-remember mechanism on spreading, *Eur. Phys. J. B*, **62** (2008), 247–255. https://doi.org/10.1140/epjb/e2008-00139-4

19. L. Zhao, X. Qiu, X. Wang, J. Wang, Rumor spreading model considering forgetting and remembering mechanisms in inhomogeneous networks, *Phys. A*, **392** (2013), 987–994. https://doi.org/10.1016/j.physa.2012.10.031

20. J. Chen, H. Ma, S. Yang, SEIOR rumor propagation model considering hesitating mechanism and different rumor-refuting ways in complex networks, *Mathematics*, **11** (2023), 283. https://doi.org/10.3390/math11020283

21. A. El Bhih, R. Ghazzali, S. Ben Rhila, M. Rachik, A. El Alami Laaroussi, A discrete mathematical modeling and optimal control of the rumor propagation in online social network, *Discrete Dyn. Nat. Soc.*, **2020** (2020), 4386476. https://doi.org/10.1155/2020/4386476

22. N. Ding, G. Guan, S. Shen, L. Zhu, Dynamical behaviors and optimal control of delayed $S^2IS$ rumor propagation model with saturated conversion function over complex networks, *Commun. Nonlinear Sci. Numer. Simul.*, **128** (2024), 107603. https://doi.org/10.1016/j.cnsns.2023.107603

23. H. Guo, X. Yan, J. Zhang, Modeling and simulation of rumor propagation and optimal control strategy based on social positive reinforcement, *Eur. Phys. J. Plus*, **140** (2025), 49. https://doi.org/10.1140/epjp/s13360-024-05953-y

24. D. Sharma, A. Shah, C. Gopalappa, A multi-agent reinforcement learning framework for public health decision analysis, *Healthcare Anal.*, **8** (2025), 100436. https://doi.org/10.1016/j.health.2025.100436

25. G. Liu, H. Li, L. Xiong, Y. Chen, A. Wang, D. Shen, Reinforcement learning for mitigating malware propagation in wireless radar sensor networks with channel modeling, *Mathematics*, **13** (2025), 1397. https://doi.org/10.3390/math13091397

26. S. Shen, X. Hao, Y. Shen, H. Xu, J. Dong, Z. Fang, Deep-reinforcement-learning-based botnet propagation control in the social internet of things, *IEEE Int. Things J.*, **12** (2025), 27481–27495. https://doi.org/10.1109/JIOT.2025.3562583

27. H. Lin, C. Tian, L. Chen, D. Liao, Y. Wang, Y. Hua, Model-based reinforcement learning for containing malware propagation in wireless radar sensor networks, *Actuators*, **14** (2025), 434. https://doi.org/10.3390/act14090434

28. D. Zhan, L. F. Toso, J. Anderson, Coreset-based task selection for sample-efficient meta-reinforcement learning, *2025 IEEE 64th Conference on Decision and Control (CDC)*, Rio de Janeiro, Brazil, 2025. https://doi.org/10.1109/CDC57313.2025.11312186

29. M. Raissi, P. Perdikaris, G. E. Karniadakis, Physics-informed neural networks: a deep learning framework for solving forward and inverse problems involving nonlinear partial differential equations, *J. Comput. Phys.*, **378** (2019), 686–707. https://doi.org/10.1016/j.jcp.2018.10.045

30. M. Kim, Y. Kim, Y. Kim, Physics-informed neural networks for optimal vaccination plan in SIR epidemic models, *Math. Biosci. Eng.*, **22** (2025), 1598–1633. https://doi.org/10.3934/mbe.2025059

31. A. Zhong, B. She, P. E. Paré, A physics-informed neural networks-based model predictive control framework for SIR epidemics, *IEEE Open J. Control Syst.*, **5** (2025), 31–48. https://doi.org/10.1109/OJCSYS.2025.3641369

32. G. C. Calafiore, C. Novara, C. Possieri, A time-varying SIRD model for the COVID-19 contagion in Italy, *Annu. Rev. Control*, **50** (2020), 361–372. https://doi.org/10.1016/j.arcontrol.2020.10.005

33. P. van den Driessche, J. Watmough, Reproduction numbers and sub-threshold endemic equilibria for compartmental models of disease transmission, *Math. Biosci.*, **180** (2002), 29–48. https://doi.org/10.1016/S0025-5564(02)00108-6


AIMS Press